Vortices of mesoscopic rings in an external magnetic field: Phenomenological Ginzburg-Landau theory

Liang-Ma Shi, Ling-Feng Zhang, Hao Meng, Hong-Wei Zhao, Guo-Qiao Zha, and Shi-Ping Zhou
Department of Physics, Shanghai University, 99 Shangda Road, Shanghai 200444, People's Republic of China
(Received 4 January 2009; revised manuscript received 4 March 2009; published 20 May 2009)

Vortex states in mesoscopic superconducting rings are investigated by the phenomenological Ginzburg-Landau theory in the presence of an externally applied magnetic field. We obtain the cylindrical symmetric giant vortex states (GVS) by solving an eigenvalue problem and minimizing the system free energy. Ground state transitions between GVS and multivortex states are found as system dimensions and magnetic field vary. Metastability and negative flux jump associated with quantum size effect and proximity effect are revealed. Also, We find that the superconducting state and the normal state can alternately appear with external field increasing.

DOI: 10.1103/PhysRevB.79.184518 PACS number(s): 74.78.Na, 74.20.De

I. INTRODUCTION

The recent progress of modern nanofabrication technologies resulted in an increase in interest in the mesoscopic sample[1–9] whose size is comparable to the penetration depth λ or the coherence length ξ. The behavior of such superconductors is strongly influenced by the samples shape and size. Yampolskii *et al.*[8,10] first studied the mesoscopic disks[1] and cylinder[9] in the framework of the phenomenological Gingburg-Landau theory.[11,12] After that, Zhou *et al.*[13–15] investigated the mesoscopic thin rings. They extended Yampolskii's approach from one boundary to double boundaries. Baelus *et al.*[16] investigated the mesoscopic sphere and mesoscopic cones,[17] and a three-dimensional approach was studied.

For axially symmetric mesoscopic samples,[1,8–10,16–18] the superconducting states can be subdivided into two different types. In the first case, the Cooper-pair density is axially symmetric inside the sample such as the Meissner state and the giant vortex state (GVS). In the second case, the axial symmetry is broken and a vortex cluster is formed inside the sample. It is called as the multivortex state (MVS), and this state usually appears at larger sample size as compared to the giant vortex state. GVS and MVS have been recently observed in mesoscopic superconductors.[19–22]

The mesoscopic ring has been one of the most popular objects which has more complex boundary and structure in comparison with a simple connected dish or a sphere sample. Actually, the ring can be viewed as multiply connected. The behavior of such structures in an external magnetic field (H) is strongly influenced by the sample shape and may lead to various superconducting states and different phase transitions between them. In the present paper, we consider three-dimensional mesoscopic superconducting rings placed in an externally applied magnetic field. Solving Gingburg-Landau equations, we obtain various stable and the metastable vortex states. The stability of the giant and multivortex states are studied as ring size and magnetic field vary.

This paper is organized as follows. In Sec. II, we present the theoretical approach on which our numerical result is based. In Sec. III, we present eigenvalue and free-energy diagram as a function of magnetic field for different ring dimensions. In Sec. IV, we consider linear combinations of two different giant vortex states in order to find possible multivortex states and the stability region of the giant vortex states. Our results are summarized in Sec. V.

II. THEORETICAL APPROACH

We consider a mesoscopic superconducting ring with inner radius R_i and circle radius r. The ring geometry is shown in Fig. 1 together with the coordinate system we choose. The ring is surrounded by vacuum with an external uniform magnetic field $\vec{H} \equiv \overrightarrow{He_Z}$ along the z axis.

According to Ginzburg and Landau, the Gibbs free energy of the superconduction near the critical temperature T_c can be expanded in powers of Cooper pairs $|\psi(\vec{r})|^2$,

$$F_s - F_n = \int dV \left\{ \alpha(T)|\psi|^2 + \frac{1}{2}\beta(T)|\psi|^4 + \frac{\hbar^2}{2m^*}\left|\left(\vec{\nabla} - i\frac{2\pi}{\Phi_0}\vec{A}\right)\psi\right|^2 - \frac{1}{4\pi}(\vec{\nabla}\times\vec{A} - \vec{H})\cdot\vec{H} \right\}. \tag{1}$$

We measure the distance in units of the coherence length $\xi = \hbar/\sqrt{2m[-\alpha(T)]}$, the vector potential in $c\hbar/2e\xi(T)$, the magnetic field in $H_{c2} = c\hbar/2e\xi(T)^2$, the order parameter in $\psi_0 = \sqrt{-\alpha(T)/\beta}$, and the free energy in $F_0 = \alpha(T)^2/2\beta$, where

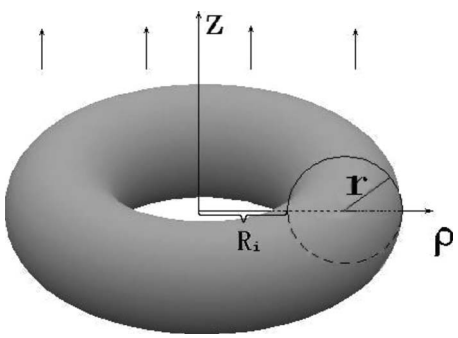

FIG. 1. Coordinate system and the circular ring in the presence of an applied field.

H_c is the thermodynamical critical field. In terms of these dimensionless units, the free energy becomes

$$F = 2\int dV\left\{-|\psi|^2 + \frac{1}{2}|\psi|^4 + |(\vec{\nabla} - i\vec{A})\psi|^2\right\}. \quad (2)$$

Here, magnetic shielding effect has not been accounted. This assumption is applicable for mesoscopic superconductors and large κ values.

By minimizing the Gibbs free energy with respect to $\psi(\vec{r})$, one obtains the Ginzburg-Landau equation and the boundary condition

$$(-i\vec{\nabla} - \vec{A})^2\psi = \psi - \psi|\psi|^2, \quad (3)$$

$$\vec{n}\cdot(\vec{\nabla} - i\vec{A})\psi|_{onS} = 0, \quad (4)$$

We use the cylindrical coordinates $\vec{r}=(\rho,\theta,z)$ where ρ is the radial distance from the cylinder axis z and θ is the azimuthal angle and choose the gauge $\vec{A}=(H\rho/2)\vec{e_\theta}$ which satisfies the London gauge $\nabla\cdot\vec{A}=0$. Their order parameter should be cylindrically symmetric that is expressed as

$$\Psi(\rho,\theta,z) = e^{iL\theta}\psi(\rho,z). \quad (5)$$

We introduce the $\hat{L}$ operator

$$\hat{L} = -\frac{1}{\rho}\frac{\partial}{\partial\rho}\left(\rho\frac{\partial}{\partial\rho}\right) - \frac{\partial^2}{\partial z^2} + \left(\frac{L}{\rho} - \frac{H\rho}{2}\right)^2 - 1. \quad (6)$$

The free-energy expression Eq. (2) reduces to

$$F = 2\pi\int_{-r}^{r} dz \int_{R_i+r-\sqrt{r^2-z^2}}^{R_i+r+\sqrt{r^2-z^2}} \rho d\rho\left(\psi^*\hat{L}\psi + \frac{1}{2}|\psi|^4\right). \quad (7)$$

$\hat{L}$ has a eigenvalue problem

$$\hat{L}\psi_{L,n}(\rho,z) = \Lambda_{L,n}\psi_{L,n}(\rho,z), \quad (8)$$

where L is the vorticity and $n=0,1,2,\ldots$, enumerates the different states for the same vorticity L. $\Lambda_{L,n}$ is the eigenvalue for fixed vorticity L and inner ring radius R_i and circler radius r. We restrict ourselves to $n=0$ because these states are known to give the major contribution and hereafter drop the n in $\psi_{L,n}(\rho,z)$ in favor of a short notation, such that $\psi_L(\rho,z)$ stands for $\psi_{L,n=0}(\rho,z)$. Similarly, Λ_L is short for $\Lambda_{L,n=0}$.

Then a general expression of the order parameter is in this basis

$$\Psi(\rho,\theta,z) = \sum_{L}^{N} C_L\psi_L(\rho,z)\exp(iL\theta), \quad (9)$$

where N is the maximum vorticity L. Substituting Eq. (9) into the free-energy expression of Eq. (7) gives F as a function of the complex coefficients $\{C_L\}$. To obtain the equilibrium vortex configurations, F must be minimized with respect to the linear solution free parameters $\{C_L\}$,

$$\frac{\partial F}{\partial C_L} = 0 \quad \text{and} \quad \frac{\partial F}{\partial C_L^*} = 0, \quad (10)$$

and the stability of the solution verified. If the state is stable, then its Hessian matrix should be positive definite. We consider two cases that just a single term which describe the GVS and a two-component order parameter which describe the MVSs in Eq. (9).

A. GVS states

Here

$$\Psi(\rho,\theta,z) = C_L\psi_L(\rho,z)\exp(iL\theta). \quad (11)$$

The free energy of a single-component state is

$$F = 2\Lambda_L C_L^2 b_L + C_L^4 a_L, \quad (12)$$

where $a_L = 2\pi\int_{-r}^{r}dz\int_{R_i+r-\sqrt{r^2-z^2}}^{R_i+r+\sqrt{r^2-z^2}}\rho d\rho\psi_L(\rho,z)^4$ and $b_L = 2\pi\int_{-r}^{r}dz\int_{R_i+r-\sqrt{r^2-z^2}}^{R_i+r+\sqrt{r^2-z^2}}\rho d\rho\psi_L(\rho,z)^2$. The coefficient C_L is a constant to be determined by imposing on conditions of Eq. (10) and Hessian Matrix $\frac{\partial^2 F}{\partial C_L^2} > 0$. One then obtains

$$C_L = \pm\sqrt{-\Lambda_L\frac{b_L}{a_L}}, \quad (13)$$

and for the free energy

$$F = -\Lambda_L^2\frac{b_L^2}{a_L}. \quad (14)$$

B. MVS states

Here

$$\Psi(\rho,\theta,z) = C_{L1}\psi_{L1}(\rho,z)\exp(iL1\theta) + C_{L2}\psi_{L2}(\rho,z)\exp(iL2\theta). \quad (15)$$

The free energy of a two-component state is

$$F = C_{L1}^4 A_{L1} + C_{L2}^4 A_{L2} + 4C_{L1}^2 C_{L2}^2 A_{L1,L2} + 2\Lambda_{L1}C_{L1}^2 B_{L1} + 2\Lambda_{L2}C_{L2}^2 B_{L2}, \quad (16)$$

where $A_{Li} = 2\pi\int_{-r}^{r}dz\int_{R_i+r-\sqrt{r^2-z^2}}^{R_i+r+\sqrt{r^2-z^2}}\rho d\rho\psi_{Li}(\rho,z)^4$ and $B_{Li} = 2\pi\int_{-r}^{r}dz\int_{R_i+r-\sqrt{r^2-z^2}}^{R_i+r+\sqrt{r^2-z^2}}\rho d\rho\psi_{Li}(\rho,z)^2$ $(i=1,2)$; $A_{L1,L2} = 2\pi\int_{-r}^{r}dz\int_{R_i+r-\sqrt{r^2-z^2}}^{R_i+r+\sqrt{r^2-z^2}}\rho d\rho\psi_{L1}^2(\rho,z)\psi_{L2}^2(\rho,z)$. In general, C_L is a complex number in Eq. (9), for our two-component state $\{C_{L1},C_{L2}\}$ is, however, a pair of real numbers. By minimizing the free energy with respect to C_{L1} and C_{L2},

$$\frac{\partial F}{\partial C_{Li}} = 0, \quad (i=1,2), \quad (17)$$

and its Hessian matrix

$$\left.\frac{\partial^2 F}{\partial C_{Li}\,\partial(C_{Lj})}\right|_{C_{Li}=C_{Li}^{(0)},C_{Lj}=C_{Lj}^{(0)}} \quad (i,j=1,2) \quad (18)$$

must be positive definite, where $C_{Li}^{(0)}, C_{Lj}^{(0)}$ are solutions of Eq. (17).

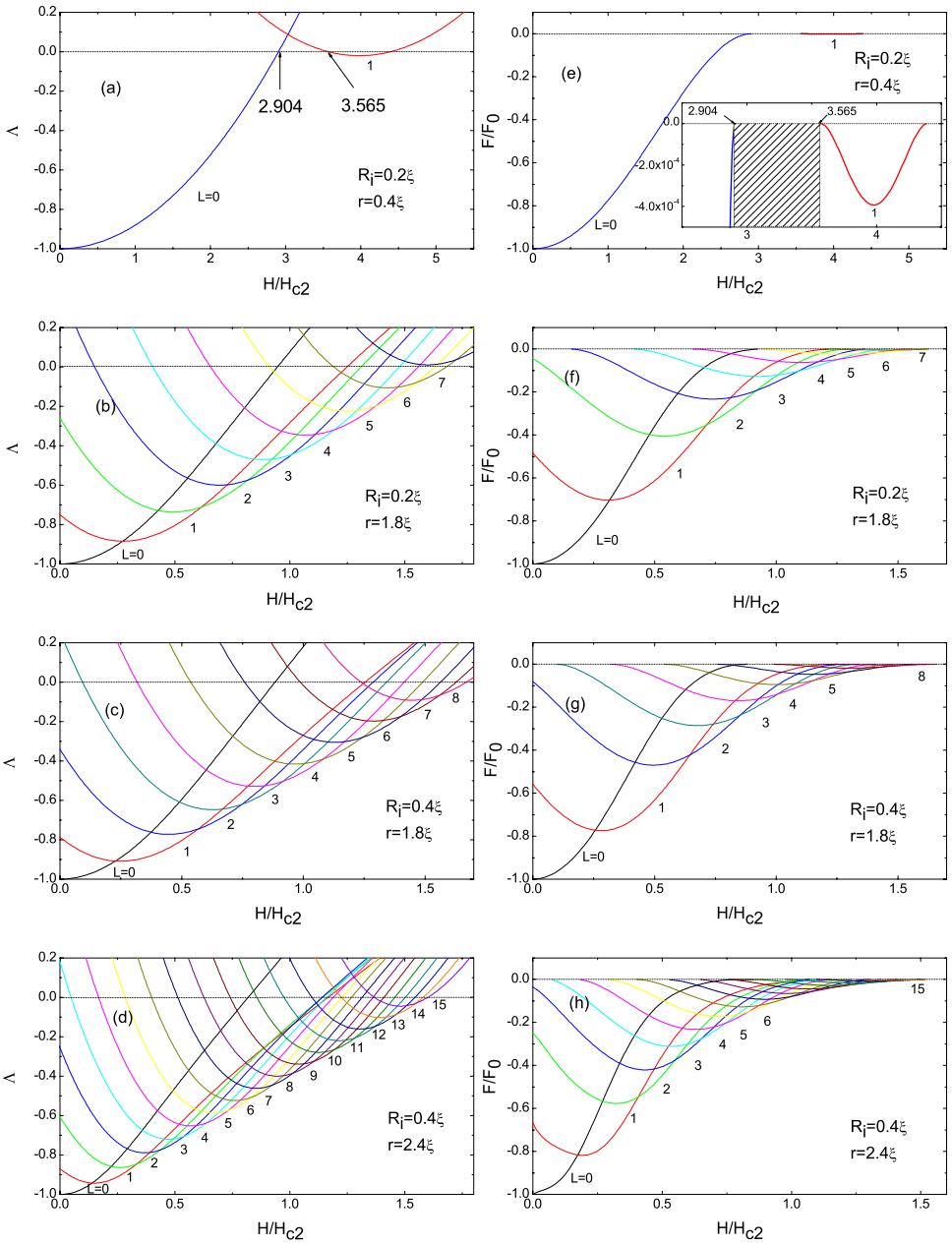

FIG. 2. (Color online) Eigenvalue [(a)–(d)] and free energy [(e)–(h)] vs applied magnetic field plots for different ring. The inset is the enlargements of some of the curves in a limited H region.

We obtain the solutions of $\{C_{L1}, C_{L2}\}$,

$$C_{L1} = \pm \left(\frac{-\Lambda_{L1} A_{L2} B_{L1} + 2\Lambda_{L2} A_{L1} B_{L2}}{A_{L1} A_{L2} - 4A_{L1,L2}^2} \right)^{1/2}, \quad (19)$$

$$C_{L2} = \pm \left(\frac{-\Lambda_{L2} A_{L1} B_{L2} + 2\Lambda_{L1} A_{L2} B_{L1}}{A_{L1} A_{L2} - 4A_{L1,L2}^2} \right)^{1/2}, \quad (20)$$

and for the free energy,

$$F_{L1,L2} = \frac{-\Lambda_{L1}^2 A_{L2} B_{L1}^2 - \Lambda_{L2}^2 A_{L1} B_{L2}^2 + 4\Lambda_{L1}\Lambda_{L2} A_{L1,L2} B_{L1} B_{L2}}{A_{L1} A_{L2} - 4A_{L1,L2}^2}. \quad (21)$$

III. GIANT VORTEX STATES

Since we are interested in a solution that is invariant under rotation around the z axis, the problem then reduces to two dimensions. For the two-dimensional problem, the sample area was meshed into $N \times N$ grids. Discrete equation were obtained by using a finite-difference procedure from Eq. (8), which leads to an algebra equation of $N \times N$ orders for the wave function $\psi_{(i,j)}$ with i, and $j = 1, 2, \ldots, N$. It should be noted that once a wave function outside of the sample area is involved as the grid (i, j) approaching to sample's boundary, the boundary conditions of Eq. (4) must be imposed on so that the algebra equation set is self-consistent. Eigenvalues and functions are evaluated numerically.

First, we calculate the eigenvalue and the free energy versus magnetic field of the giant vortex for various ring dimensions. Figure 2 shows the eigenvalue and the free energy

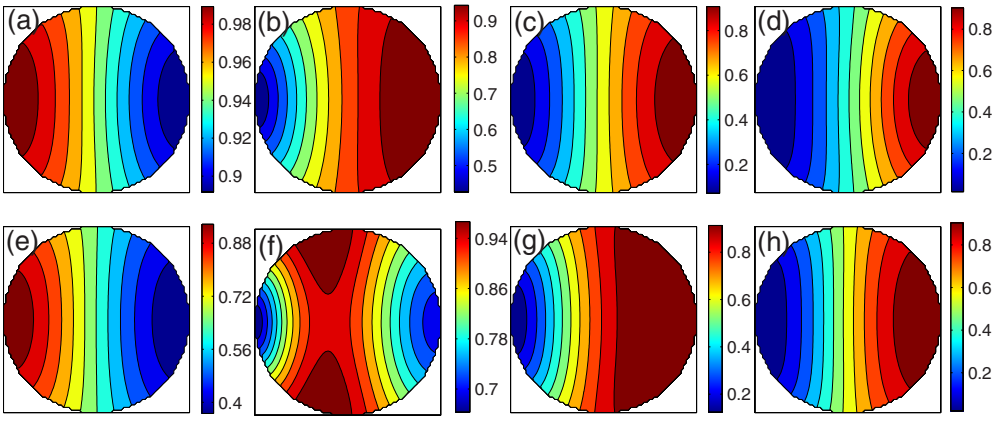

FIG. 3. (Color online) Contour plots of the Cooper-pair density in the (ρ,z) plane for a 0.4–1.8 ring for vorticity $L=0$ [(a) and (e)], $L=1$ [(b) and(f)], $L=2$ [(c) and (g)], and $L=3$ [(d) and (h)] at applied magnetic fields $H/H_{c2}=0.2$ [(a)–(d)] and 0.60 [(e)–(h)]. The vertical axis (the z direction) corresponds to the direction of the applied magnetic field, while the horizontal axis corresponds to the radial direction ρ. Blue to red means Cooper-pair density range from minimum to maximum. The color bars beside indicate the value of Cooper-pair density.

versus magnetic field diagrams, with Figs. 2(a)–2(d) for the eigenvalues and Figs. 2(e)–2(h) for the free energy. Ground states with more vorticities appear as R_i or r increases, e.g., $L=1$ for ring dimension $0.2-0.4[R_i=0.2\xi,\ r=0.4\xi]$, $L=7$ for $0.2-1.8[R_i=0.2\xi,\ r=1.8\xi]$, $L=8$ for $0.4-1.8[R_i=0.4\xi,\ r=1.8\xi]$, and $L=15$ for $0.4-2.4[R_i=0.4\xi,\ r=2.4\xi]$, respectively. While increasing r, but fixed R_i, more vortex states become stable in Figs. 2(a)–2(d), since more vortex states have eigenvalues with $\Lambda<0$ and the nucleation field $H_{\rm nuc}$ for possible maximum vorticity L state decreases. Also, the $L\rightarrow L+1$ ground-state transition field decreases. A similar conclusion can be drawn when increasing R_i with fixed r. Note that the nucleation field $H_{\rm nuc}$ of $L=0$ state is calculated to be $2.904H_{c2}$ as shown in Fig. 2(a). This implies that when $H<2.904H_{c2}$, the sample remains in the Meissner state. We believe this is due to the finite quantum effect that provides a surface carrier for field penetration. Although there is a hole in the center of ring, the magnetic field cannot penetrate through the hole until it arrives $2.904H_{c2}$. This characterizes superconducting proximity effect. Also, notice that the nucleation field $H_{\rm nuc}$ of vorticity $L=1$ state with the 0.4–2.4 ring exceed $H_{\rm nuc}$ of $L=2,3$ in Fig. 2(d).

Figures 2(e)–2(h) show that for a certain H, there may exist more than one stable GVS. The lowest one in free energy is the ground state and the other ones are metastable states. The dotted horizontal line is a guide for the eyes to indicate the normal state. In Fig. 2(e), obviously, when $2.904H_{c2}<H<3.656H_{c2}$, the system shifts to the normal state. Note that both giant states are the ground states and the multivortex states never exist. We have the remarkable result that the superconducting state and the normal state (shaded regions in the inset) cyclically appear as the value of field increasing.

The order parameter of the giant vortex state is given by Eq. (11). In order to learn the order parameter of the giant vortex state distributions, Fig. 3 shows a contour plot of the GVS cooper-pair density in the (ρ,z) plane for a 0.4–1.8 ring for vorticity $L=0$ [(a) and (e)], $L=1$ [(b) and (f)], $L=2$ [(c) and (g)], and $L=3$ [(d) and (h)] at applied magnetic fields $H/H_{c2}=0.2$ [(a)–(d)] and 0.60 [(e)–(h)]. Blue to red means Cooper-pair density from minimum to maximum. The color bars beside indicate the value of Cooper-pair density. For $L=0$, no vortex is present in the ring and the cooper-pair density is maximum near the inner side of ring, while the superconducting density is suppressed from the outer side of the ring with increasing magnetic field. For larger L, magnetic field penetrates the hole of the ring and a giant vortex is formed. The highest Cooper-pair density may be found in the outer side of ring or in the ring. In Fig. 3(f), we find that the Cooper-pair density is suppressed from the inner and outer sides of the ring.

Next, we calculate the Cooper-pair density and the phase of the order parameter in the xy plane at $z=0$ for the same parameters as in Figs. 3(e)–3(h). Contour plots of the Cooper-pair density are given in Figs. 4(a)–4(d). For $L=0$, the Cooper-pair density is highest in the inner side of the ring, while it decreases with increasing ρ. When $L>0$, the Cooper-pair density is low in the inner side of the ring, as the magnetic field penetrates the hole of the ring. The phase of the order parameter is an important tool to identify the vor-

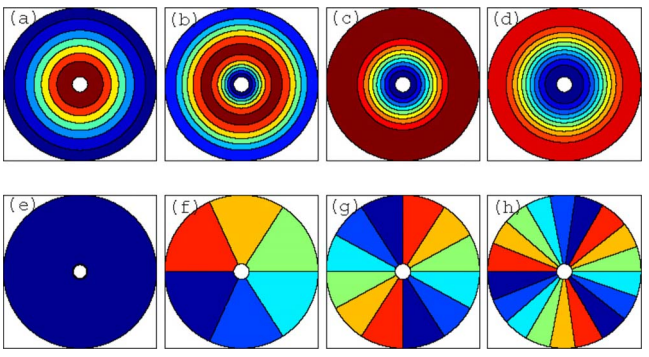

FIG. 4. (Color online) [(a)–(d)] Contour plots of the Cooper-pair density in the xy plane, i.e., $z=0$, for the 0.4–1.8 ring for vorticity $L=0$, 1, 2, and 3 at $H/H_{c2}=0.6$. [(e)–(h)] Phase of the order parameter for the same parameters as in (a)–(d). Blue to red means Cooper-pair density range from minimum to maximum, whereas for (e)–(h), it indicates $0-2\pi$ range.

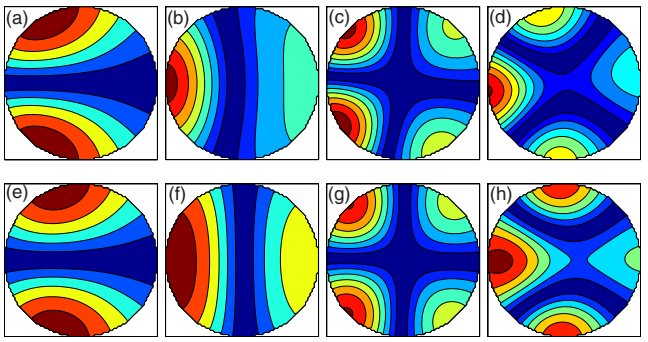

FIG. 5. (Color online) Contour plots of the Cooper-pair density of the first ($n=1$), second ($n=2$), third ($n=3$), and fourth ($n=4$) excited states for $L=0$ [(a)–(d)] and $L=1$ [(e)–(h)] at $H/H_{c2}=0.8$. Blue to red means Cooper-pair density varying from minimum to maximum.

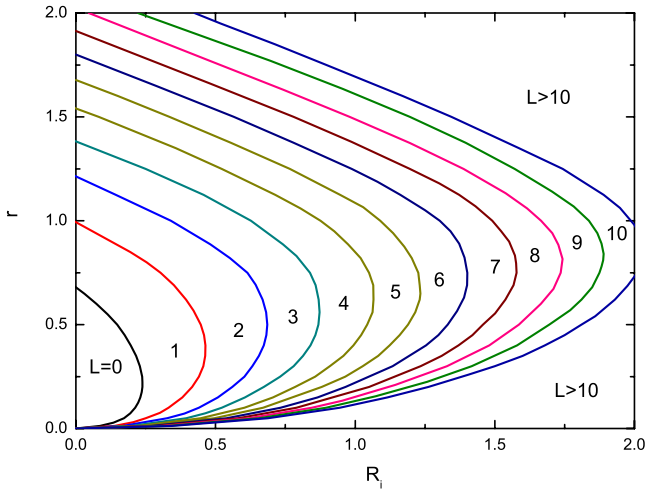

FIG. 6. (Color online) The maximum vorticity with inner radius R_i and ring radius r versus the applied field H.

ticity because it is equal to $L\times\theta$ at any point inside the ring. Thus a state with vorticity L is identified by the presence of L, consecutive red to blue hues. In Figs. 4(e)–4(h), the phase of the order parameter in the xy plane at $z=0$ is shown for the giant vortex states with vorticity $L=0$, 1, 2, and 3, corresponding to the situations of Figs. 4(a)–4(d). In these figures, a blue to red tour means $0-2\pi$ in the phase.

Up to now, we restricted ourselves to $n=0$ for the lowest-energy state In Eq. (8). Now, we investigate the excited $n>0$ states. For the $n>0$ state, there are no stable states since all the states have positive eigenvalues for all magnetic fields and thereby called as excited state, whereas for the $n=0$ states it corresponds to the lowest radial state which $\Psi_{L,n}(\rho,z)$ has no node as a function of ρ with a negative eigenvalue. This is the reason why we restrict ourselves to $n=0$ in Eq. (8). Figure 5 shows contour plots of the Cooper-pair density of the first ($n=1$), second ($n=2$), third ($n=3$), and fourth ($n=4$) excited states for $L=0$ [(a)–(d)] and $L=1$ [(e)–(h)] at $H/H_{c2}=0.8$. Blue to red means the Cooper-pair density varies from minimum to maximum.

We present the phase diagram for giant vortex states as the inner radius R_i and ring radius r in the range of $[0,2\xi]$ in Fig. 6. For a given dimension, the maximum vorticity $L_{\max}$ corresponds to the highest angular momentum quantum of a GVS that is able to render a negative eigenvalue for the operator $\hat{L}$. We see that $L_{\max}$ increases with R_i for fixed r, while it is nonmonotonic with r for fixed R_i. This can be understood as a result of the competition between superconducting phase and normal state. When the ratio of normal area over superconducting size is small (say, $R_i/\xi=1$ and $r/\xi=0.02$), the system shows a very weak superconductivity. Magnetic flux can then site in the hole as many as possible, thereby a high $L_{\max}$ value. Slightly enlarging ring radius r, superconducting phase enhanced, which would expel some fluxons out of the hole via the proximity effect, leading to somewhat a less $L_{\max}$. For an even large ring radius, however, the total fluxons become significantly large and are squeezed into the hole because of an even enhanced superconductivity or the Meissner effect, resulting to an increasing in $L_{\max}$, as if a re-entrant process.

IV. MULTIVORTEX STATES

We use a two-component order parameter expression which is able to describe MVS. We use the notation ($L1$-$L2$) to indicate the MVS whose order parameter is formed by ψ_{L1} and ψ_{L2}. State $L1$ (wave function ψ_{L1}) and state $L2$ (wave function ψ_{L1}) are the giant states with vorticities $L1$ and $L2$. The two-component approximation is good in case there are vortices in the hole of the center and at most in the ring, an approximation suitable for small mesoscopic superconductors. In that case, a MVS described by a two-component state with an angular momentum of $L1$ and $L2$ has vortices equal to the larger one of $L1$ and $L2$.

We calculate the free energy of all the (meta)stable state in a superconducting ring with dimensions of 0.2–0.4, 0.2–

TABLE I. The MVS states of various ring dimensions we study.

Dimension (R_i-r)	0.2–0.4	0.2–1.8	0.4–1.8	0.4–2.4
	no	$(0-L), L=3,4,5$	$(0-L), L=3,4,5,6$	$(0-L), L=3,4,\ldots,10$
		$(1-L), L=4,5,6$	$(1-L), L=4,5,6,7$	$(1-L), L=4,5,\ldots,13$
			$(2-L), L=6,7,8$	$(2-L), L=6,7,8,\ldots,13$
			$(3-L), L=8$	$(3-L), L=7,8,\ldots,13$
				$(4-L), L=9,10,\ldots,13$
				$(5-L), L=11,12,13$
MVS				$(6-L), L=12,13$

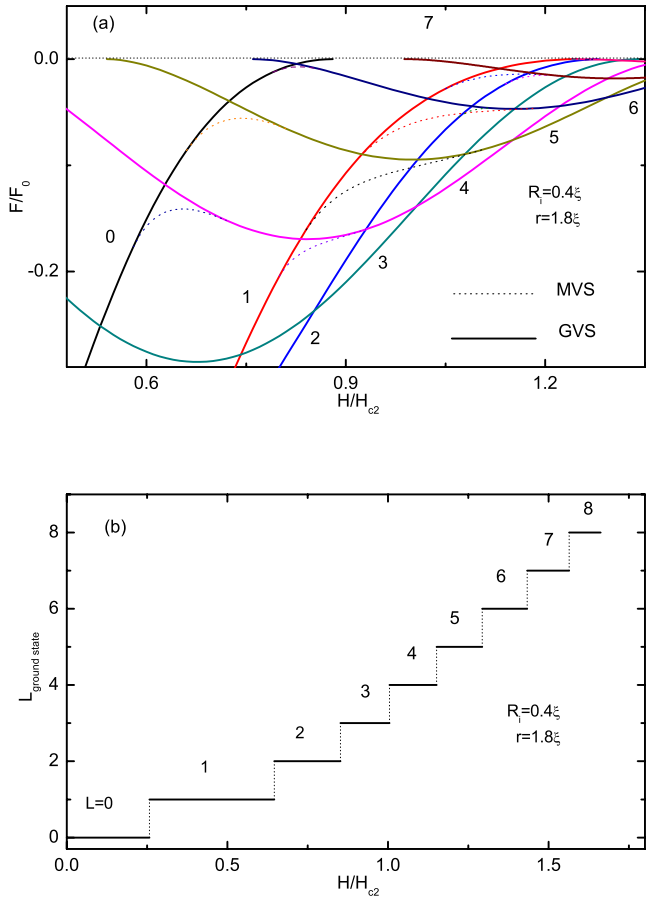

FIG. 7. (Color online) (a) Plot of the free energy of the 0.4–1.8 vs the applied magnetic field. (b) The vorticity of the ground state vs the applied magnetic field.

1.8, 0.4–1.8, and 0.4–2.4 as a function of the applied magnetic field. According to the stable conditions, the MVS states in Table I are stable states. It is clear that MVS states are getting more with the increasing of the ring dimension.

Figure 7(a) shows the free energy of several states versus the H field. The GVS curves are solid lines, whereas the MVS curves are represented by a dotted line. We find that there are no MVS states existing in the ground states for the 0.4–1.8 ring. The (0–3) and (3–8) curves are not visible since both states exist in a small H region. Figure 7(b) shows the vorticity of the ground state as a function of the field.

Figure 8(a) shows the free energy as a function of H for the 0.4–2.4 ring, while Fig. 8(b) is a zoom of the certain H region. It is clear that the $(1-L)(L=4-9)$ state is a ground state. Note that the $L=0$, 1, 2, 3, and $9,10,\ldots,15$ giant vortex states are the ground state, whereas $L=4$, 6, 7, and 8 are not. For $L=9$, the ground state is first characterized by the (1–9) state and then by the giant vortex $L=9$ state. To show the variation in the ground state as a function of the applied magnetic field, we present Fig. 8(c). When the ground state is a giant vortex state, the result is given by black curves, while for the $(1-L)$ state, we indicate the ground state by red curves.

To get further insight into the nature of the MVS state, we investigate the Cooper-pair density in the $z=0$ plane of the ring. In Fig. 9, contour plots of the Cooper-pair density of all

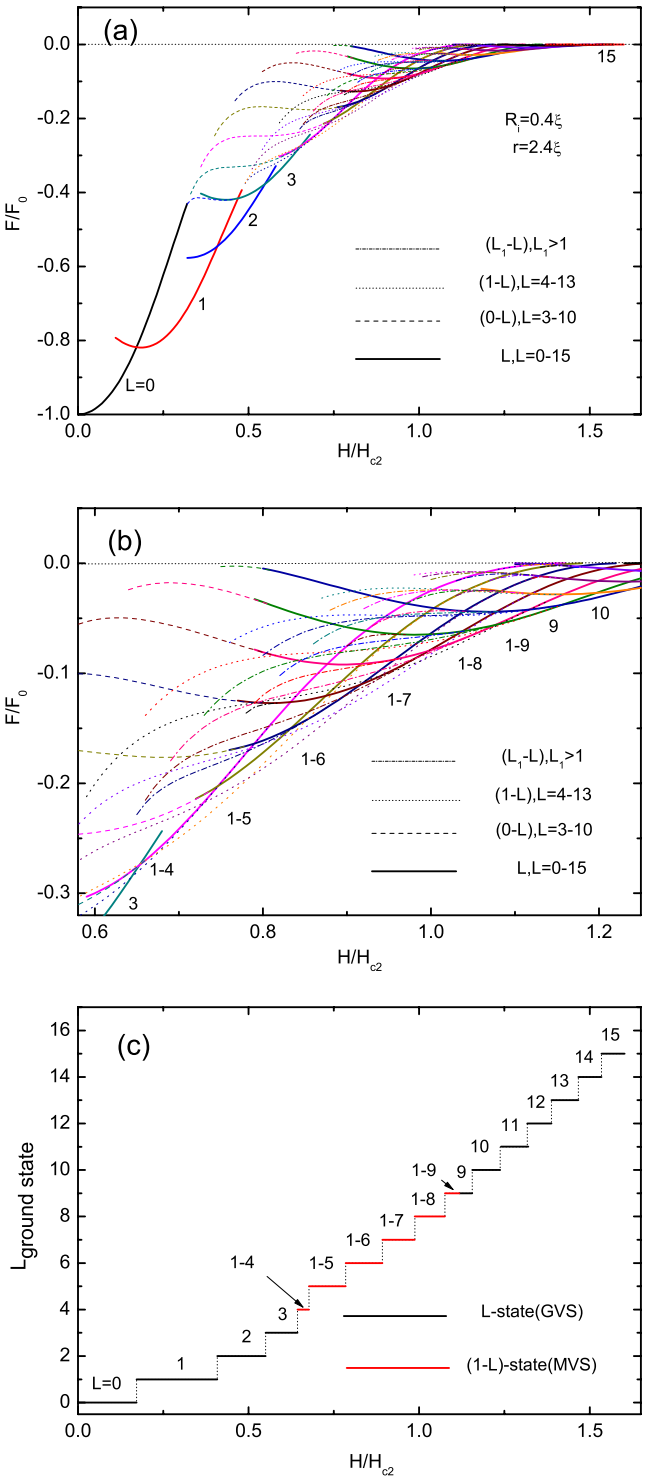

FIG. 8. (Color online) (a) is the free energy of the 0.4–2.4 ring as a function of the applied magnetic field. (b) is a zoom of the certain field H region of (a). (c) is the vorticity of the ground state as a function of the applied magnetic field.

multivortex states for the 0.4–1.8 ring. Figures 9(a)–9(d) correspond to the $(0-L)(L=3,4,5,6)$ states at $H/H_{c2}=0.55$, 0.60, 0.75, and 0.80. For the $(0-L)(L=3,4,5,6)$ states, there are L single vortices which are arranged on a shell with no vortex in the center hole. Figures 9(e)–9(h) correspond to the $(1-L)(L=4,5,6,7)$ states at $H/H_{c2}=0.85$, 0.95, 1.00, and

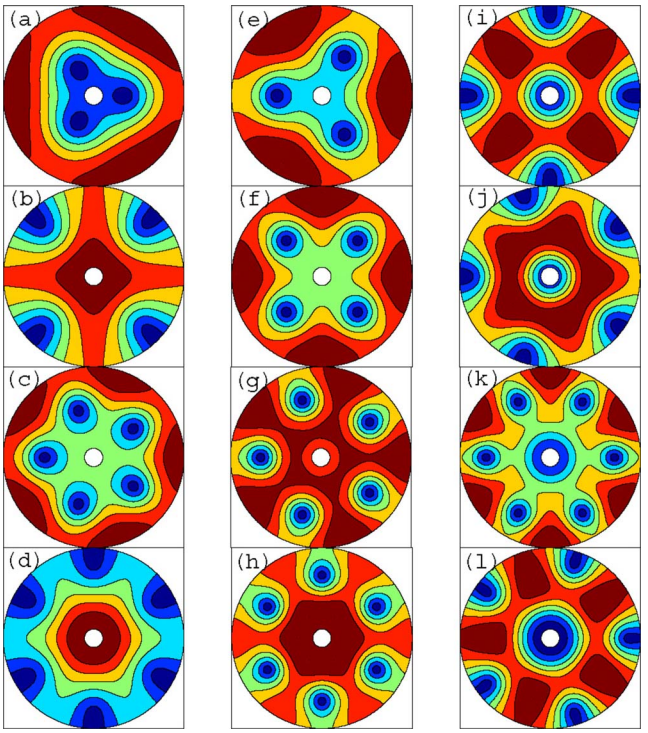

FIG. 9. (Color online) Contour plots of the Cooper-pair density in the $z=0$ plane of the 0.4–1.8 for the (0–3), (0–4), (0–5), and (0–6) state at $H/H_{c2}=0.55$, 0.60, 0.75, and 0.80 [(a)–(d)]; (1–4), (1–5), (1–6), and (1–7) state at $H/H_{c2}=0.85$, 0.95, 1.00, and 1.10 [(e)–(h)]; (2–6), (2–7), (2–8), and (3–8) state at $H/H_{c2}=1.05$, 1.15, 1.25, and 1.30 [(i)–(l)].

1.10. For the $(1-L)(L=4,5,6,7,8)$ states, there are L vortices with $(L-1)$ forming a shell and a vortex in the center hole. Figures 12(i)–12(l) correspond to the $(2-L)(L=6,7,8)$ and (3–8) states at $H/H_{c2}=1.05$, 1.15, 1.25 and 1.30. For the $(2-L)(rmL=6,7,8)$ [Figs. 9(i)–9(k)] states $L-2$ of them are located on a shell with a giant vortex in the center hole with vorticity 2. For the (3–8) [Fig. 9(l)] state, there is a giant vortex in the center hole with vorticity three while five of them located on a shell.

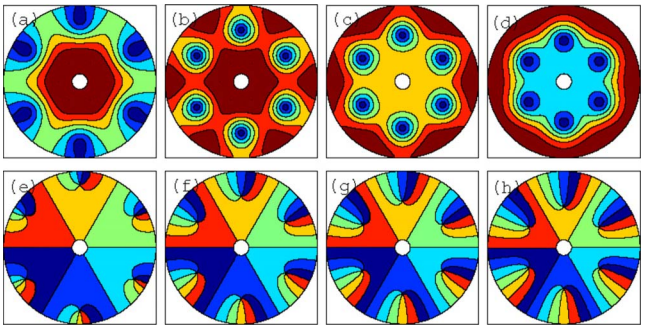

FIG. 10. (Color online) [(a)–(d)] The contour plots of the Cooper-pair density distribution for the (1–7) state with the 0.4–2.4 at the field $H/H_{c2}=1.05$, 1.10, 1.15, and 1.20. [(e)–(h)] Phase of the order parameter for the same parameters as in (a)–(d). Blue to red means Cooper-pair density range from minimum to maximum, whereas for (e)–(h), it indicates $0-2\pi$ range.

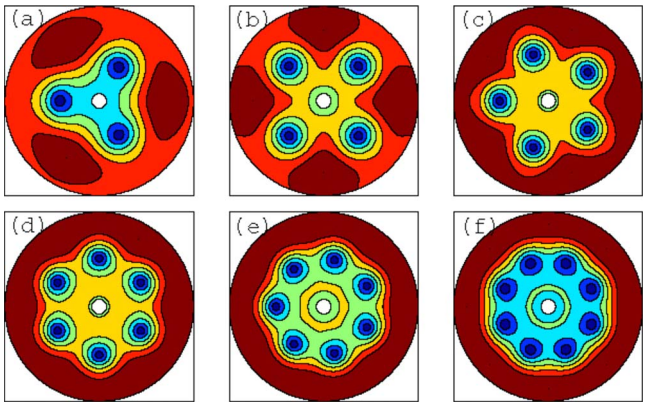

FIG. 11. (Color online) [(a)–(f)] The Cooper-pair density distribution of the ground states of the MVS in the $z=0$ plane with the 0.4–2.4 for the $(1-L)(L=4,5,\ldots,9)$ state at the field $H/H_{c2}=0.66$, 0.69, 0.81, 0.92, 1.01 and 1.09. Blue to red means Cooper-pair density range from minimum to maximum.

To investigate the effects of the magnetic field on a MVS vortex configuration, the MVS (1–7) is examined at different fields $H/H_{c2}=1.05$, 1.10, 1.15, and 1.20. Figures 10(a)–10(d) display the corresponding plots at the fields. One can obtain that the six vortices shift toward the center with increasing H value. When encircling a single vortex, the phase of the order parameter changes with 2π. From Figs. 10(e)–10(h), it is clear that there is a vortex in the center hole, the other six vortices at the shell. To further understand the ground states of the MVS, Fig. 11 shows the Cooper-pair density of ground states of the MVS distribution in the $z=0$ plane for the 0.4–2.4 ring.

Curiously, we find that there are two regimes for the free-energy cure of the MVS (1–4) state which one demonstrates the ground state in the low magnetic field H region, while another the metastable state in the high magnetic field H region in Fig. 8(b). To understand this, Fig. 12 shows the free energy of the MVS (1–4) state as a function of the applied magnetic field. The inset is the enlargement of some of the curve selected H region.

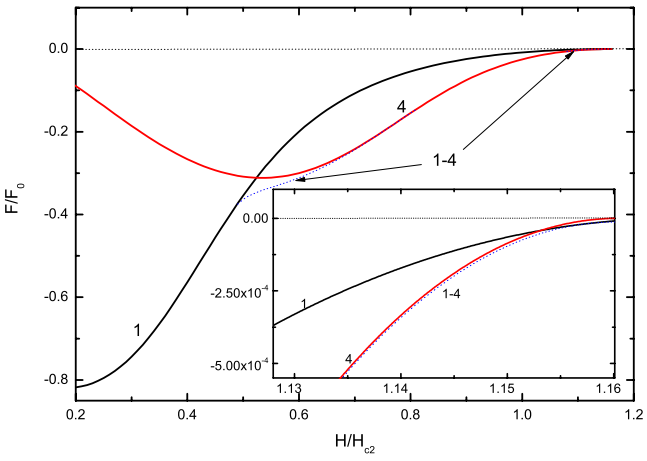

FIG. 12. (Color online) The free energy of the MVS (1–4) state as a function of the applied magnetic field. The inset is the enlargement of some of the curve in a high H region.

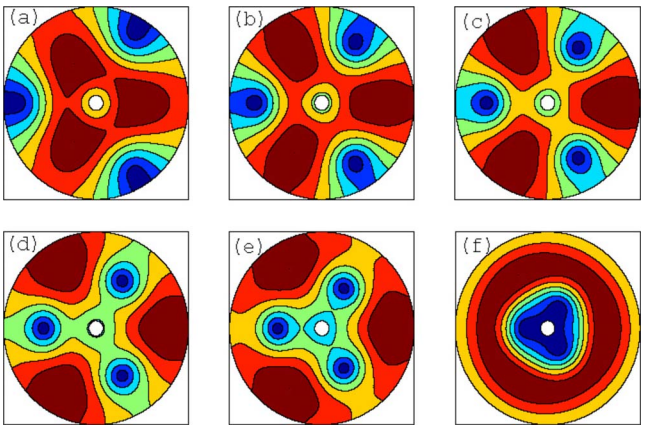

FIG. 13. (Color online) Contour plots of the Cooper-pair density in the $z=0$ plane with the 0.4–2.4 ring for the (1–4) state at $H/H_{C2}=0.49$, 0.50, 0.51, 0.54, 0.60, and 0.80 [(a)–(f)].

To show the difference of them, we plot Figs. 13 and 14. Figures 13(a)–13(f) show clearly that the three vortices move toward the center with increasing magnetic field. From Figs. 14(a)–14(e), however, the three vortices move outside away from the center with increasing magnetic field. It clear that there is negative flux jump with increasing magnetic field (see Ref. 22). From Figs. 14(f)–14(j), we know that a vortex settles down in the hole.

Due to the boundary of the circular ring, the spatial distribution of the vortices will change when going away from the $z=0$. Figure 15 shows the three-dimensional distribution of the Cooper-pair density in a superconducting circular ring with the 0.4–1.8 at $H/H_{c2}=0.65$, 0.80, 1.25, and 1.30 for the (0–5), (1–5), (2–8), and (3–8) states. Note that the diameters of the vortices in these figures are different from the vortices in the two-dimensional contour plots above. Here, we show the isosurfaces where the Cooper-pair density has a fixed but low value. The value of the Cooper-pair density in Fig. 10(a) is 0.002, where (b) is 0.012, (c) is 0.00018, and (d) is 0.0003. Figure 15(a) shows the (0–5) state, where five vortices on a shell with no vortex are in the center hole. One can obtain that all vortices bend toward the outer boundary when $z \neq 0$. Figure 15(b) shows the (1–5) state, where one vortex is in the center hole, which is surrounded by four vortices on a shell. Since the central vortex is not visible, we zoom the value of the Cooper-pair density to 0.012. Figures 15(c) and

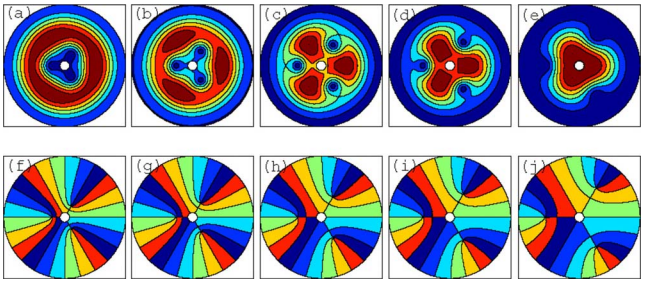

FIG. 14. (Color online) Contour plots of the Cooper-pair density [(a)–(e)] and phase of the order parameter [(f)–(j)] in the $z=0$ plane with the 0.4–2.4 for the (1–4) state at $H/H_{C2}=1.09$, 1.12, 1.52, 1.55, and 1.57.

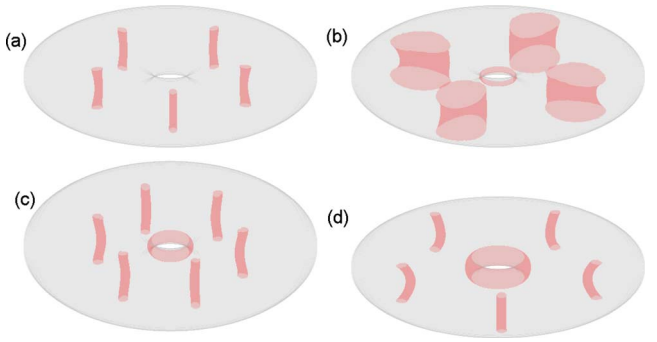

FIG. 15. (Color online) (a)–(d) show three-dimensional figures of the (0–5), (1–5), (2–8), and (3–8) states of the 0.4–1.8 ring.

15(d) show the (2–8) and (3–8) states, where a central giant vortex is the single vortices. From these figures, it is also clear that the radius of the giant vortex decreases with increasing $|z|$ in the center hole.

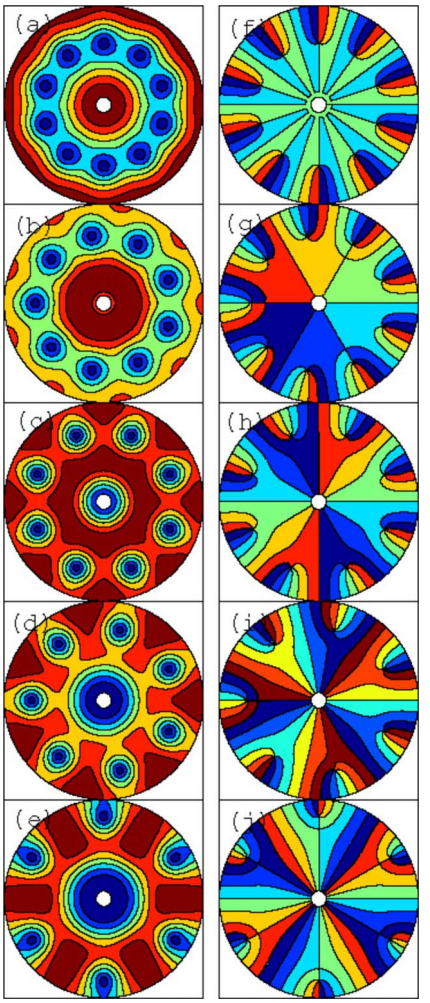

FIG. 16. (Color online) (a)–(e) show plots of the Cooper-pair density of the 0.4–2.8 ring for the (meta)stable MVS $(L1-10)(L1=0,1,2,3,4)$ at the field $H/H_{c2}=0.77$, 0.81, 0.86, 0.92, and 0.94. Blue to red means Cooper-pair density range from minimum to maximum. (e)–(h) show plots of order parameter phase of (a)–(e), and blue to red indicates $0-2\pi$ range.

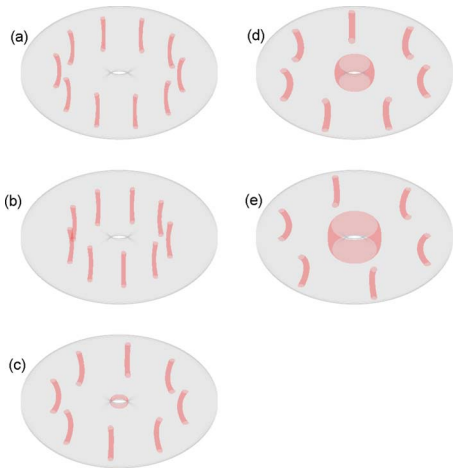

FIG. 17. (Color online) The plots of the vortex configuration of ring with the 0.4–2.4 for the (meta)stable MVS $(L1-10)(L1=0,1,2,3,4)$ at the field $H/H_{c2}=0.77$, 0.81, 0.86, 0.92, and 0.94 [(a)–(e)].

For the $(L1\text{-}L2)$ MVS, we have studied the MVS with $L1$ fixed. Now, we focus on some MVSs which share the same $L2$ vorticity. For example, Fig. 16 is the contour of Cooper-pair density and order parameter phase for the $(L1-10)(L1=0,1,2,3,4)$ MVSs at $H/H_{c2}=0.77$, 0.81, 0.96, 0.92, and 0.94 with the 0.4–2.4 ring. Figures 16(f)–16(j) show that there are $L1$ vortices in the center hole.

Figures 17(a)–17(e) are the spatial distribution of the Cooper-pair density in a superconduction ring with the 0.4–2.4 for the corresponding same parameters as in Figs. 16(a)–16(e). Here, we show the isosurfaces where the Cooper-pair density has a fixed value. The cooper-pair density in Figs. 17(a)–17(c) are 0.003 when (d) is 0.002 (e) is 0.001. It is clear that the radius increases with $L1$ increasing where the radius of the giant vortex in center hole decreases with increasing $|z|$.

V. CONCLUSIONS

In conclusion, we study the stable and metastable vortex states in mesoscopic superconducting rings with different dimensions by using the phenomenological Ginzburg-Landau theory. First, we find that with increasing r and fixed R_i or increasing R_i and fixed r, more vortex states stabilize, while the superconduction and/or normal transition field decrease. Although there is a hole in the ring, the magnetic field which value arrives high cannot penetrate in the hole. We obtain that the ring we study has the superconducting proximity effect. Also, we get the markable result that the superconducting state and the normal state alternately appear as the field varies.

Second, we take the two-component order parameter of the different giant vortex states to obtain approximate solutions of the nonlinear Ginzburg-Landau theory. We find that multivortex states are ground state in mesoscopic ring that we studied. Also, the metastable state has negative flux jump with increasing field.

ACKNOWLEDGMENTS

This work was supported by the National Natural Science Foundation of China (Grant No. 60671042) and by Shanghai leading academic discipline project under Grant No. S30105. H.W.Z. acknowledges the Innovation Funds for Graduates of Shanghai University (2008), China (Grant No. shucx080121). G.Q.Z. acknowledges the Innovation Funds of Shanghai University, China.

[1] V. A. Schweigert, F. M. Peeters, and P. S. Deo, Phys. Rev. Lett. **81**, 2783 (1998).
[2] S. Pan, E. Hudson, and J. Davis, Appl. Phys. Lett. **73**, 2992 (1998).
[3] J. G. Rodrigo, H. Suderow, and S. Vieira, Eur. Phys. J. B **40**, 483 (2004).
[4] H. Suderow, E. Bascones, A. Izquierdo, F. Guinea, and S. Vieira, Phys.Rev.B **65**, 100519(R) (2002).
[5] A. Kohen, T. Proslier, T. Cren, Y. Noat, W. Sacks, H. Berger, and D. Roditchev, Phys. Rev. Lett. **97**, 027001 (2006).
[6] M. Poza, E. Bascones, J. G. Rodrigo, N. Agraït, S. Vieira, and F. Guinea, Phys. Rev. B **58**, 11173 (1998).
[7] J. Rodrigo, H. Suderow, and S. Vieira, Phys. Status Solidi B **237**, 386 (2003).
[8] S. V. Yampolskii, B. J. Baelus, F. M. Peeters, and J. Kolacek, Phys. Rev. B **64**, 144511 (2001).
[9] G. F. Zharkov, V. G. Zharkov, and A. Yu. Zvetkov, Phys. Rev. B **61**, 12293 (2000).
[10] B. J. Baelus, S. V. Yampolskii, F. M. Peeters, E. Montevecchi, and J. O. Indekeu, Phys. Rev. B **65**, 024510 (2001).
[11] P. Lipavsky, J. Kolacek, K. Morawetz, and E. H. Brandt, Phys. Rev. B **66**, 134525 (2002).
[12] V. R. Misko, V. M. Fomin, and J. T. Devreese, Phys. Rev. B **64**, 014517 (2001).
[13] S. P. Zhou, Y. M. Shi, B. H. Zhu, and G. Q. Zha, Phys. Rev. B **73**, 174503 (2006).
[14] G. Q. Zha, S. P. Zhou, B. H. Zhu, and Y. M. Shi, Phys. Rev. B **73**, 104508 (2006).
[15] B. H. Zhu, S. P. Zhou, Y. M. Shi, G. Q. Zha, and K. Yang, Phys. Rev. B **74**, 014501 (2006).
[16] B. J. Baelus, D. Sun, and F. M. Peeters, Phys. Rev. B **75**, 174523 (2007).
[17] Y. Chen, M. M. Doria, and F. M. Peeters, Phys. Rev. B **77**, 054511 (2008).
[18] R. Benoist and W. Zwerger, Z. Phys. B: Condens. Matter **103**, 377 (1997).
[19] A. Kanda, B. J. Baelus, F. M. Peeters, K. Kadowaki, and Y. Ootuka, Phys. Rev. Lett. **93**, 257002 (2004).
[20] I. V. Grigorieva, W. Escoffier, J. Richardson, L. Y. Vinnikov, S. Dubonos, and V. Oboznov, Phys. Rev. Lett. **96**, 077005 (2006).
[21] I. V. Grigorieva, W. Escoffier, V. R. Misko, B. J. Baelus, F. M. Peeters, L. Y. Vinnikov, and S. V. Dubonos, Phys. Rev. Lett. **99**, 147003 (2007).
[22] A. K. Geim, S. V. Dubonos, I. V. Grigorieva, K. S. Novoselov, F. M. Peeters, and V. A. Schweigert, Nature (London) **407**, 55 (2000).